Protic Ionic Liquids: Preparation, Characterization, and Proton Free Energy Level Representation†

Jean-Philippe Belieres and C. Austen Angell*

Department of Chemistry and Biochemistry, Arizona State University, Tempe Arizona 85287-1604

Received: November 15, 2006; In Final Form: January 23, 2007

We give a perspective on the relations between inorganic and organic cation ionic liquids (ILs), including members with melting points that overlap around the borderline 100 °C. We then present data on the synthesis and properties (melting, boiling, glass temperatures, etc.) of a large number of an intermediate group of liquids that cover the ground between equimolar molecular mixtures and ILs, depending on the energetics of transfer of a proton from one member of the pair to the other. These proton-transfer ILs have interesting properties, including the ability to serve as electrolytes in solvent-free fuel cell systems. We provide a basis for assessing their relation to aprotic ILs by means of a Gurney-type proton-transfer free energy level diagram, with approximate values of the energy levels based on free energy of formation and pK_a data. The energy level scheme allows us to verify the relation between solvent-free acidic and basic electrolytes, and the familiar aqueous variety, and to identify neutral protic electrolytes that are unavailable in the case of aqueous systems.

Introduction

Ionic liquids (ILs), and particularly room-temperature ILs, have attracted much attention in recent years, and many new applications beyond green chemistry continue to be found. They are the low-melting relatives of molten salts whose place in the history of chemical innovation goes back to the foundations of chemistry. Many of the elements of our periodic table were first revealed by the electrolysis of one or other "ionic liquid" in the form of molten halides.[1] The difference is only that, by use of large compound cations to reduce the coulomb attractions to anions and complicated shapes to confuse the ion packing problem, the crystalline state of the system is sufficiently destabilized for melting to occur near to or below ambient.[2]

Because of the differences in properties between the average IL and the average high-temperature molten salt (e.g., 2 orders of magnitude in conductivity and fluidity, non-Arrhenius vs Arrhenius temperature dependences of these properties, etc.), and because of the differences in their applications in industrial chemistry (e.g., winning of aluminum vs solvent function for synthetic inorganic chemistry) there has developed some sort of schism between the different branches of the IL field. We commence this article with a reminder of the essential artificiality of this division and then draw attention to a further division in the field, which is of a qualitatively different type.

In Figure 1a, we make an Arrhenius plot comparison of the viscosities of various members of the inorganic and organic cation family of molten salts, and then in Figure 1b show the same data in scaled Arrhenius plot form using the calorimetric glass temperature, T_g, to scale the temperature. T_g serves as a cohesive energy parameter,[2] and Figure 1b shows that when scaled for cohesive energy it is no longer possible to tell the difference between the salts with inorganic cations and those with molecular (organic) cations. The same type of scaling (using *ideal* glass temperatures) was used long ago to relate molten salt hydrates to anhydrous molten salts.[3]

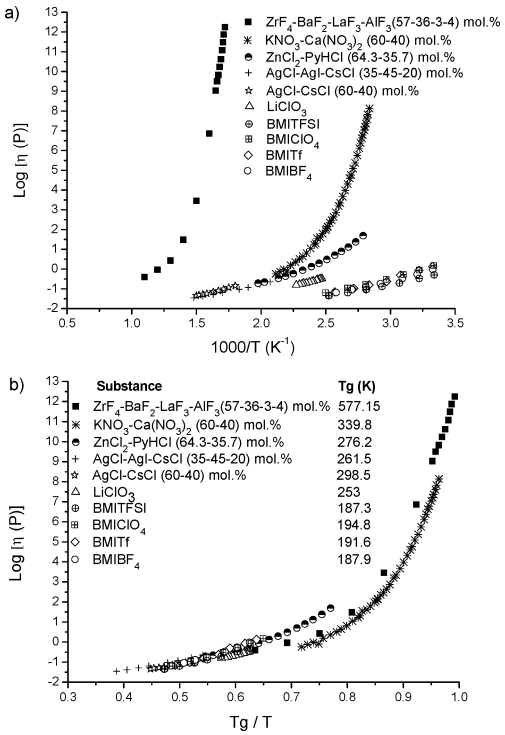

Figure 1. (a) Arrhenius plot of viscosity data on molten salts and on ILs. (b) T_g-scaled Arrhenius plot of the same data, showing underlying similarity.

While applications of molecular cation ILs have been dominated by their solvent function,[4,5] there are now developing new applications in which the electrical charges on the ions are specifically employed. A good example is that of electrolytes for photoelectrochemical (solar) cells.[6] Recently a new and potentially important application of ILs has been recognized—that of the electrolyte in a fuel cell.[2,7,8] This is an application which requires the presence of a special type of ionic liquid—one in which the cation provides a vehicle for exchangeable protons. We refer here to the ILs formed by proton transfer

† Part of the special issue "Physical Chemistry of Ionic Liquids".

* To whom correspondence should be addressed. Phone: (480) 965-7217. Fax: (480) 965-2747. E-mail: caa@asu.edu.

10.1021/jp067589u CCC: $37.00
Published on Web 04/07/2007

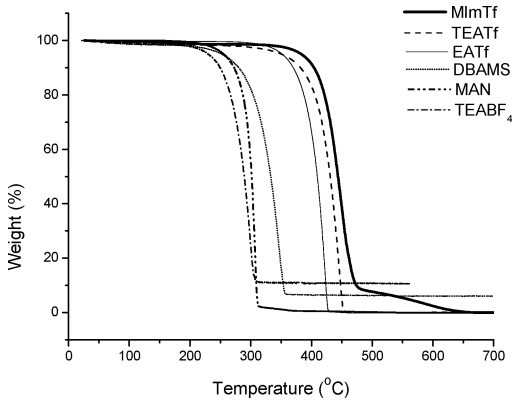

Figure 2. TG scans of a selection of PILs, showing their varying thermal stabilities.

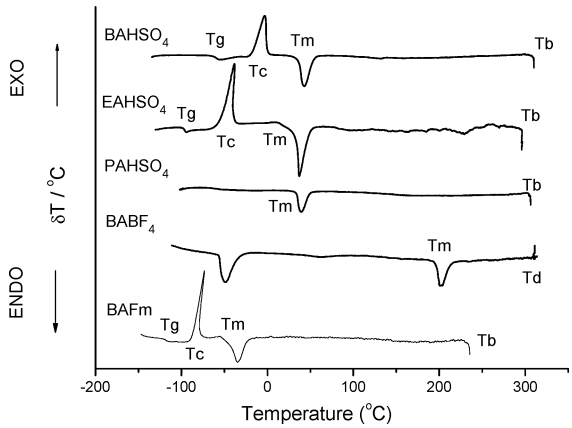

Figure 3. DTA scans for some PILs from this study. Arrows indicate successive thermal events, glass transition temperature T_g, crystallization temperature T_c, melting point T_m, and boiling point T_b (endothermic) or decomposition temperature Td (exothermic).

from a Brönsted acid to a Brönsted base, i.e., by the method used to make the first recorded ambient temperature ionic liquid nearly a century ago.[9] These are ILs of a qualitatively different type, because their ionicity is adjustable, by virtue of the different driving forces for the proton-transfer that can be chosen.

Protic ILs (PILs), such as pyridinium chloride,[10] have long been used as sources of highly basic chloride ions for spectroscopic studies[11] and also as a means of obtaining low-melting salt mixtures,[12] but such studies have been made mainly by physical chemists interested in accessing the "low-temperature domain" of liquid behavior. Since "ILs" became attractive as synthetic media, many protic ILs have been reported, particularly by Ohno and co-workers.[13−15] To provide ILs that were unequivocally ionic, Ohno and co-workers used proton transfer from a very powerful acid, hydrogen bis-trimethylsulfonyl imide, HTFSI, the conjugate base of which is an anion that is well known for promoting low melting points. In a more recent study, our own group has explored the relationship between this proton-transfer process and the nature of the acid transferring the proton.[16,17] We have demonstrated[16] that the melting points and glass transition temperatures tend to be lower, and the conductivities tend to be higher, for the protic than for the aprotic ILs, even though the conductivity at a given viscosity tends to be the same (Walden rule).

Applications of nonaqueous protonated Brönsted bases in fuel cell technology have been focused on the imidazole molecule, the use of which as a carrier of protons in a fuel cell was introduced in 1998.[18] In the latter studies the carrier was incorporated with polymeric anions as a membrane. More recently,[7,19] neat protic ILs were shown to serve well in place of acid or base electrolytes in simple bubbler cells. The most surprising finding[2,20,21] is that the polarization of the oxygen electrode, always a major problem for the efficiency of fuel cells, can be almost overcome in an ionic liquid fuel cell with high area catalyst surface cathodes when the right protic IL is used. The slope of the Tafel plot (cell voltage vs log current) that is proportional to the energy barrier opposing the electron-transfer process proves to be almost zero.

This latter finding has stimulated a major synthetic and testing effort in our group, involving the preparation of protic salts utilizing a wide variety of acid + base combinations in the effort to find systematic trends in the properties of the resulting salts and particularly in the open-circuit voltages of H_2/O_2 fuel cells utilizing the salts as electrolytes. The results of the latter study will be reported elsewhere.[21] Here we present and discuss the findings for the basic physical and electrochemical properties of the protic salts, some 103 in total number.

Experimental Section

Materials. Anhydrous trifluoromethanesulfonic acid (triflic acid, HTf, 99%) was obtained from Alfa Aesar. Anhydrous difluorophosphoric acid was obtained from SynQuest Labs Inc. Anhydrous formic acid (HFm, 98%) was obtained from Fluka. Analytical reagents phosphoric acid (85%, ACS grade) and sulfuric acid (95−98%, ACS grade) were obtained from Mallinckrodt Chemicals. Nitric acid (68−70%, GR ACS grade) was obtained from EMD Chemicals Inc. The acids methanesulfonic acid (70 wt.% in water), tetrafluoroboric acid (48 wt.% in water), and hydrofluoric acid (HF, 48%) and the bases methylamine (MA, 40 wt.% in water), ethylamine (EA, 70 wt.% in water), propylamine (PA, 99+%), butylamine (BA, 99.5%), tert-butylamine (tBA, 99.5+%), 2-methoxyethylamine (MOEA, 98%), 3-methoxypropylamine (MOPA, 99%), dimethylamine (DMA, 40 wt.% in water), diethylamine (DEA, 99+%), dibutylamine (DBA, 99.5+%), *N*-methylbutylamine (MBA, 96%), *N*-ethylbutylamine (EBA, 99%), trimethylamine (TMA, 99.5%), triethylamine (TEA, 99.5%), tributylamine (TBA, 99%), *N*,*N*-dimethylethylamine (DMEA, 99%), aniline (An, ACS reagent >99.5%), 2-fluoropyridine (FPy, 98%), imidazole (Im, 99+%), 1-methylimidazole (MIm, 99+%), and 1,2-dimethylimidazole (DMIm, 98%) were obtained from Aldrich Chemical Co. All chemicals were used as received.

PILs are formed by proton transfer between a Brönsted acid and a Brönsted base. An equimolar amount of acid and base, either neat or in an aqueous solution, are reacted together. Since these reactions are very exothermic, the dropwise addition of the acid to the amine was carried out by cooling the amine solution to −78 °C, using an acetone/dry ice bath. The mixture was then stirred at room temperature for several hours. To ensure a complete reaction, a slight excess of amine was used and then removed along with the water by heating at 80 °C in vacuum using a rotary evaporator. The same general process may be used for the synthesis of all PILs, but when amines of higher molecular weight are employed, there is a risk of contamination of the product by residual amines. When necessary, adequate purification procedures were applied.[4,22] The product was then dried at 80 °C for 2 days in a vacuum oven containing phosphorus pentoxide P_2O_5 to remove any excess water. For most of our syntheses, the reactions were carried out without any solvent at all. The structure of each PIL was identified by NMR spectroscopy and/or by elemental analysis. The complete removal of water and the absence of other −OH-containing species were confirmed by the absence of O−H stretching bands from

TABLE 1: Glass Transition Temperatures for Selected PILs of This Study[a]

cation	HCOOH ($R = 1.69$)	H_2F_2 ($R = 1.72$)	HNO_3 ($R = 1.79$)	H_2SO_4 ($R = 1.90$)	H_3PO_4 ($R = 2.00$)	CH_3SO_3H ($R = 2.24$)[b]	HBF_4 ($R = 2.30$)	CF_3SO_3H ($R = 2.70$)
NH_4		n.d.[b]	n.d.	−65.6	−23.3			
MA	−108.2	−104.1	n.d.	n.d.	−28.8	n.d.	n.d.	
EA	−127.5	−100.3	−91.5[c]	−96.4	−31.3	n.d.	n.d.	n.d.
BA	−120.1			−63.4	−33.3	−89.6	n.d.	
DMA	n.d.	−111		n.d.	−36.8	−95		
DBA	−116.4			n.d.	−15.6	−49	n.d.	
TEA				−100.1	−34.4	−96.5	n.d.	n.d.
DMEA	−121.1			−91.4		n.d.		
Im			n.d.[e]				n.d.	n.d.
Mim			n.d.[e]				n.d.	45.8
Eim			n.d.[e]				−87[e]	n.d.[e]
DMIm			n.d.[e]				−74.7	n.d.[e]
EMIm			n.d.[e]				−88	

[a] Anion radius in angstroms. [b] Reference 36. [c] Not detected. [d] Extrapolated from ref 38. [e] Reference 37.

3400 to 3800 cm^{-1} in the infrared spectra of the final melts. The PILs were then stored in an argon atmosphere glovebox (VAC, $O_2 < 1$ ppm and $H_2O < 1$ ppm).[23] In the case of EAN, a Karl Fisher water titration device was used to determine that the water content was less than 0.025 wt.%.

The thermal transitions of interest to this work were determined using a simple home-made DTA instrument[24] comprising a twin thermocouple setup employing twin digital voltmeters with microvolt sensitivity, interfaced to a laboratory computer for readout and recording purposes. One reason for choosing the DTA technique over the better-controlled differential scanning calorimetry technique is that, with DTA, samples can be taken to their boiling points without endangering the instrumentation. Boiling points, where the total pressure of all species in the vapor-phase reaches 1 atm, provide a useful metric of the energy of the proton-transfer process and of course fix the temperature range of application of the ionic liquid in question. The boiling points are signaled by a sharp endothermic effect as the enthalpy of vaporization (involving relocation of proton on the acid) is absorbed.

The DTA sample holder assembly consists of an aluminum temperature-smoothing block with two wells to contain Pyrex glass sample and reference tubes (3 mm outside diameter) into which thermocouples could be inserted. The aluminum block holder was heated from −150 to +400 °C by two 200-W heating cartridges, symmetrically disposed. The heating rate was controlled by a Barnant Co. temperature controller, model 68900-11 interfaced to a computer. For reproducibility purposes, it is important to ensure that the thermocouple and container are consistently located at the same depth in the block. The two K-type thermocouples are connected in opposition so that the $\sim\mu$V voltage differences between the sample and the reference can be read out. The output of the reference thermocouple was used separately to determine the temperature at which any thermal event of interest occurred. Anhydrous alumina was used as reference material. About 0.2 mL of the solution was loaded into the DTA sample cell. The thermocouples, protected by fine glass capillary tubes, were immersed to 50% depth in the sample and reference material, respectively. A plug was made by wrapping Teflon tape around the capillary tube. Samples were quenched in liquid nitrogen, inspected for state of vitrification, and then scanned during warm-up at 10 K/min. After appropriate calibration with melting point standards, this simple instrument is able to define melting points with an accuracy and precision of ±1 °C.

Ionic Conductivities. Ionic conductivities were determined from complex impedance data from an automated HP 4192A Impedance Analyzer with a frequency range of 5 Hz to 13 MHz. Heating or cooling rates were controlled by a Barnant Company Temperature Controller model 68900-11 at a standard rate of 1 °C/min. The dip-type conductivity cells for liquid electrolytes were constructed with platinum electrodes sealed in soft glass. Cell constants of about 1 cm^{-1} were determined using a standard 0.1 N KCl solution. Approximately 0.5 to 1 mL of solution was needed to perform an experiment. During measurement, the temperature of the sample was monitored using a K-type thermocouple. The conductivity was determined from the initial part of the almost frequency-independent plateau of the log(conductance) vs log f plot. Values obtained were checked against the data obtained by short extrapolation to the real axis of the usual complex impedance plot.

Density Values. Density values with an accuracy of 0.5% were measured in a VAC drybox simply by measuring the weight of the sample filling a 2-mL volumetric flask at different temperatures. Before each measurement, the flask was maintained in a heating block at the desired temperature for half an hour until the temperature was steady.

Kinematic Viscosity Measurements. Kinematic Viscosity Measurements were performed using Cannon-Ubbeholde viscometers designed for transparent liquids between 0 and 150 °C. For measurements at a higher temperature, we used a specially designed aluminum block holder heated by two 200-W heating cartridges symmetrically disposed. The heating was controlled by the same Barnant Co. system referred to above. The temperature of the sample was maintained for half an hour before measurement. $CaCl_2$ drying tubes were used to protect the samples from moisture. The precision of measurement with Cannon-Ubbeholde viscometers is determined by the reproducibility of the flow time. Because we were using a single viscometer for each sample, the precision was limited at the highest temperatures by the short flow times (<10 s). The flow times were reproducible and the standard deviation was ±0.2 s. For temperatures below 40 °C, the run times are typically 200 s or longer, hence the reading error is only 0.1% of the efflux time.

Thermogravimetric Analysis (TGA). TGA experiments were performed using a TA Instruments high-resolution TGA 2950 thermogravimetric analyzer. The samples were weighed and placed in a platinum crucible. They were then heated from room temperature to 700 °C with a heating rate usually of 10 °C/min. The sample chamber had a controllable environment to allow monitoring of the degradation under various conditions (air, oxygen, or dry nitrogen).

TABLE 2: Melting Point, T_m (°C) of Some PILs of This Study[a]

cation	HCOOH ($R = 1.69$)	H_2F_2 ($R = 1.72$)	HNO_3 ($R = 1.79$)	H_2SO_4 ($R = 1.90$)	H_3PO_4 ($R = 2.00$)	CH_3SO_3H ($R = 2.24$)[b]	HBF_4 ($R = 2.30$)	CF_3SO_3H ($R = 2.70$)
NH_4	120	125.6	163.5	116.3	193.3			225
MA	−21.7	−11.8	104.7	73.2	96.8	91	77.1	
EA	−72.9	3.5	13	31.9	109.5	112.5	152.4	172.1
BA	−46.8			33.5	113.3	131.8	198.2	
DMA	n.d.[c]	−22.9	75	40.1	117.3	122.1		
DBA	n.d.			130.9	98	42.7	212.8	
TEA				84.2	n.d.	21.6	104.3	n.d.
DMEA	n.d.			3.3		94.7		
Im							131.2	122.9
MIm			70[d]				35.8	92
EIm			31[d]				n.d.[d]	8[d]
DMIm			84[d]				31.3	119[d]
EMIm			75[d]				n.d.[d]	33[d]

[a] Anion radius in angstroms. [b] Reference 36. [c] Not detected. [d] Reference 37.

TABLE 3: Thermal Transition Temperatures for Formates

IL cation	symbol	T_g (°C)	T_c (°C)	T_m (°C)	T_b (°C)	ΔpK_a
ammonium	AFm			120		5.5
methylammonium	MAFm	−108.2	n.d.[a]	−21.7	162.1	6.9
ethylammonium	EAFm	−127.5	n.d.	−72.9	176.1	6.9
propylammonium	PAFm	−124.7	n.d.	−55.4	213.1	6.8
butylammonium	BAFm	−120.1	−89.8	−46.8	224.5	6.9
hydroxyethylammonium	HOEAFm	−88.3	n.d.	n.d.		9.1
methoxyethylammonium	MOEAFm	−103	−63.5	−22.4	209.1	5.7
methoxypropylammonium	MOPAFm	−116.4	n.d.	n.d.		6.0
dimethylammonium	DMAFm	n.d.	n.d.	n.d.	152	7.1
dibutylammonium	DBAFm	−116.4	n.d.	n.d.	234.7	7.5
dimethylethylammonium	DMEAFm	−121.1	n.d.	n.d.	187.4	6.2
ethylbutylammonium	EBAFm	−119.6	n.d.	n.d.	207.3	7.1
hydrazinium[b]		−87		44.3		4.2

[a] Not detected. [b] Reference 27.

TABLE 4: Thermal Transition Temperatures for Nitrates

IL cation	symbol	T_g (°C)	T_c (°C)	$T_{S_1 \rightarrow S_2}$ (°C)	T_m (°C)	T_b (°C)	ΔpK_a
ammonium	AN[a]	n.d.[b]	n.d.	46.7	163.5	223.8	10.5
methylammonium	MAN[a]	n.d.	n.d.	73.5	104.7	206.8	11.9
ethylammonium	EAN	−91.5[c]	−59.1	−43.8	13	240	11.9
hydroxyethylammonium	HOEAN	−87.4	−52.6	n.d.	−25.2	255.4	14.2
methoxypropylammonium	MOPAN	−82.7	n.d.	n.d.	n.d.		11.0
dimethylammonium	DMAN	n.d.	n.d.	22.4	75	explosive	12.1
methylbutylammonium	MBAN					explosive	12.2

[a] From differential scanning calorimetry data. [b] Not detected. [c] Extrapolated from ref 38.

TABLE 5: Thermal Transition Temperatures for Perchlorates

IL cation	symbol	T_g (°C)	T_c (°C)	T_m (°C)	T_b (°C)	ΔpK_a
ethylammonium	$EAClO_4$	n.d.[a]	n.d.	151.9		20.6

[a] Not detected.

Results

TGA. The thermogravimetric analysis curves of several protic ILs are shown in Figure 2. The thermal stability is seen to vary with the cation−anion combination under study, being highest when the cation is aromatic in character (methylimidazolium) and the anion a very weak base (triflate). The weight loss begins at the boiling point for low-energy proton transfers (methylammonium nitrate). For PILS formed with large proton-transfer energies (see Discussion section), boiling would only occur at very high temperatures and is pre-empted by chemical decomposition.

These TGA curves confirm the formation of protic neutral salts since we have one-step weight loss processes. In case of acid or base excess compositions, the TGA curve would show a two-step process, with the initial loss corresponding to the excess of acid or base in the system.[25]

Thermophysical Properties. Some representative DTA scans for protic ILs of this study are shown in Figure 3 to indicate the variety of signals that can be obtained for different cases and the manner in which the transition temperatures are defined from these signals.

In Tables 1−12, we record data for the various transition temperatures that can be observed: glass temperatures (if the liquids can vitrify), solid-state transition temperatures ($T_{S_1 \rightarrow S_2}$, ...), melting points, and "boiling points", respectively. Tables 1 and 2 show a single property (glass temperature T_g in Table 1, and melting point T_m in Table 2) for a variety of cations (descending), one column for each anion type, so that the trends in these two most important properties can be seen. Then, Tables 3−12 record the data on all transitions for all the cations studied, one table for each anion, the tables being ordered by increasing anion complexity, as follows:

Table 3, formates (2 oxygens);
Table 4, nitrates (3 oxygens);
Table 5, perchlorates (4 oxygens);
Table 6, tetrafluoroborates (4 fluorines);

TABLE 6: Thermal Transition Temperatures for Tetrafluoroborates

IL cation	symbol	T_g (°C)	T_c (°C)	$T_{S_1 \rightarrow S_2}$ (°C)	T_m (°C)	T_{dec} (°C)	ΔpK_a
ammonium	NH_4BF_4					dec	8.7
methylammonium	MA BF_4			−24.9	187.8		10.1
ethylammonium	$EABF_4$				152.4		10.1
butylammonium	$BABF_4$	n.d.[a]	n.d.	−55.9	198.2	310.5	10.1
tert-butylammonium	$tBABF_4$	n.d.	n.d.	−53.8	118.3	243.6	10.2
hydroxyethylammonium	$HOEABF_4$				0.5		12.4
methoxyethylammonium	$MOEABF_4$				n.d.	206.9	9.0
dibutylammonium	$DBABF_4$	n.d.	n.d.	−13	212.8	330.1	10.8
methylbutylammonium	$MBABF_4$	n.d.	n.d.	−83.9	77.1	350.3	10.4
triethylammonium	$TEABF_4$	n.d.	n.d.	−56.8	104.3	286.7	10.2
imidazolium	$ImBF_4$	n.d.	n.d.	−86.3	131.2	363.2	6.5
1-methylimidazolium	$MImBF_4$	n.d.	n.d.	−25.7	35.8	387	6.6
1,2-dimethylimidazolium	$DMImBF_4$	−74.7	−1.3	n.d.	31.3	365.2	7.9

[a] Not detected.

TABLE 7: Thermal Transition Temperatures for Triflates

IL cation	symbol	T_g (°C)	T_c (°C)	$T_{S_1 \rightarrow S_2}$ (°C)	T_m (°C)	T_b (°C)	ΔpK_a
ammonium	ATf					225[a]	23.2
anilinium	AnTf	n.d.[b]	n.d	71.3	n.d	250[a]	18.6
ethylammonium	EATf[c]	n.d	n.d	−12.9	172.1	312.1[a]	24.6
tert-butylammonium	tBATf	n.d	n.d	n.d	11.6	243.4[a]	24.7
2-fluoropyridinium	FPyTf	n.d	n.d	n.d	58.3	286	13.6
hydronium	H_3OTf	n.d	n.d	n.d	27.4	212.7	12.3
hydroxyethylammonium	HOEATf	n.d	−66	−1.6	74.8		26.9
methoxyethylammonium	MOEATf	n.d	n.d	n.d	n.d	283.5[a]	23.5
triethylammonium	TEATf	n.d	n.d	n.d	n.d	312.5[a]	24.7
1,2-dimethylimidazolium	DMImTf	n.d	n.d	n.d	115.3	298.9	22.4
imidazolium	ImTf	n.d	n.d	34	122.9	308.4	21.0
1-methylimidazolium	MImTf	45.8	56.7	78.6	92	323.5[a]	21.1

[a] Decomposes. [b] Not detected. [c] From differential scanning calorimetry data.

TABLE 8: Thermal Transition Temperatures for Methane Sulfonates

IL cation	symbol	T_g (°C)	T_m (°C)	T_{dec} (°C)	ΔpK_a
methylammonium	MAMS	n.d.[a]	91	260.2	11.2
ethylammonium	EAMS	n.d.	112.5	288.6	11.2
butylammonium	BAMS	−50	131.8	292.2	11.2
methoxyethylammonium	MOEAMS	n.d.	62.6	282.4	10.1
dimethylammonium	DMAMS	−95	122.1	278	11.4
dibutylammonium	DBAMS	−49	42.7	331.9	11.9
triethylammonium	TEAMS	−96.5	21.6	269.7	11.3
dimethylethylammonium	DMEAMS	n.d.	94.7	295.8	10.6

[a] Not detected.

Table 7, triflates (3 oxygens + perfluorinated methyl radical);

Table 8, methane sulfonates (3 oxygens + methyl radical);

Table 9, hydrogen sulfates (4 oxygens + H-bonders);

Table 10, fluorohydrogenphosphates (3 oxygens + 1 fluorine + 1 hydrogen bonder);

Table 11, dihydrogen phosphates (4 oxygens + two H-bonders);

Table 12, dianions:difluorides.

In the final column of each of Tables 3−12 we record the differences in pK_a values for the cation−anion combination ΔpK_a, based on aqueous solution measurements. These values are later used (in the Discussion section) for the construction of Gurney diagrams.

There are a small number of cases in which a glass temperature was recorded, but no subsequent crystallization and remelting was observed, suggesting that the liquid state is the stable state to very low temperatures relative to the glass temperature and hence is too viscous, when supercooled, to be able to nucleate any crystals. There are a much larger number of cases in which a melting point can be observed, but no glass transition is observed, because the liquid crystallized completely during cooling. In these cases the liquid is apparently very mobile at its melting point and has no problem in generating nuclei that then grow during cooling. For the majority of cases, both glass transitions and melting points can be measured. In these cases the two are approximately related by the "$^2/_3$ law", as will be detailed in the discussion section.

The relation between these properties, the anion and cation structures, and the ΔpK_a values in Tables 3−12 will also be taken up in the Discussion section.

Densities. Although densities can be measured very precisely, high precision was not sought in this study. Rather, we used simple rapid techniques that yielded data of precision comparable to that of the log(conductivity) for the sole purpose of obtaining equivalent conductivities to construct Walden plots. Density and molar volume data are therefore not recorded here, but are available in Supporting Information and ref 26.

Ionic Conductivities. Ionic conductivity data are collected in Figures 4 and 5, which are representative rather than exhaustive.

The conductivities can be extremely high, from >150 $mS \cdot cm^{-1}$ at 25 °C up to 470 $mS \cdot cm^{-1}$ at 100 °C, as previously reported.[16] A variety of behavior is to be seen, which will be discussed below. Among the highest are some data from a 1970 study, which have previously only been available in a thesis.[27] The system in question is the monoprotonated salt of hydrazine and formic acid.

Viscosities. The viscosities measured on these liquids, shown in Figure 6 for the same representative series as in Figures 4 and 5 are generally high compared to water as reference substance, though several cases approach waterlike values, especially at high temperatures. Some of the highest conductivities are clearly related to exceptionally low viscosities, but this relation is not clarified until the data are compared in a Walden plot (see Discussion section).

TABLE 9: Thermal Transition Temperatures for Hydrogen Sulfates

IL cation	symbol	T_g (°C)	T_c (°C)	$T_{S_1 \rightarrow S_2}$ (°C)	T_m (°C)	T_b (°C)	ΔpK_a
hydronium	H_3OHSO_4	−91.2[a]			8.5[a]	225[a]	7.3
ammonium	NH_4HSO_4	−65.6	−33	31.4	116.3	358.8[b]	18.2
methylammonium	$MAHSO_4$	n.d.[c]	n.d.	n.d.	73.2	302.3[b]	19.6
ethylammonium	$EAHSO_4$	−96.4	−54	n.d.	31.9	296.5[b]	19.6
propylammonium	$PAHSO_4$	n.d.	n.d.	n.d.	33.9	304.5[b]	19.6
butylammonium	$BAHSO_4$	−63.4	−19	n.d.	33.5	307.9[b]	19.6
tert-butylammonium	$tBAHSO_4$	n.d.	n.d.	n.d.	130.6	243.9[b]	19.7
dimethylammonium	$DMAHSO_4$	n.d.	n.d.	−61.1	40.1	310.9[b]	19.8
diethylammonium	$DEAHSO_4$	n.d.	n.d.	−43.3	77.3	301.5[b]	19.8
dibutylammonium	$DBAHSO_4$	n.d.	n.d.	16.7	130.9	283.5[b]	20.3
methylbutylammonium	$MBAHSO_4$	−79.6	−34.4	n.d.	42.2	285.8[b]	19.9
ethylbutylammonium	$EBAHSO_4$	n.d.	n.d.	−85.5	54.4	295.1[b]	19.8
trimethylammonium	$TMAHSO_4$	n.d.	n.d.	−77.7	72.9	308.9[b]	18.8
triethylammonium	$TEAHSO_4$	n.d.	n.d.	n.d.	84.2	262.8[b]	19.7
tributylammonium	$TBAHSO_4$	−57.1	−3.3	36.7	86.6	250.3[b]	19.0
dimethylethylammonium	$DMEAHSO_4$	−91.4	−34.1	n.d.	3.3	302.6[b]	19.0

[a] Reference 39. [b] Decomposes. [c] Not detected.

TABLE 10: Thermal Transition Temperatures for Fluorohydrogen Phosphates

IL cation	symbol	T_g (°C)	T_c (°C)	T_m (°C)	ΔpK_a
methylammonium	$MAHPO_3F$	−47.8	n.d.	n.d.	9.7
propylammonium	$PAHPO_3F$				9.8
butylammonium	$BAHPO_3F$	−50.1	n.d.	n.d.	10.7
dimethylammonium	$DMAHPO_3F$	−51.5	n.d.	n.d.	9.8
diethylammonium	$DEAHPO_3F$		n.d.	n.d.	9.8
dibutylammonium	$DBAHPO_3F$	−39.5	n.d.	75.7	10.3
dipropylammonium	$DPAHPO_3F$	−31.5	n.d.	n.d.	9.9
trimethylammonium	$TMAHPO_3F$	−44.5	n.d.	n.d.	8.8
triethylammonium	$TEAHPO_3F$	−59.7	n.d.	RTIL[b]	9.8
tributylammonium	$TBAHPO_3F$	−59.1	n.d.	RTIL[b]	9.0
tripropylammonium	$TPAHPO_3F$	−56.60	n.d.	30	9.0

[a] Not detected. [b] RTIL = room temperature ionic liquid.

Discussion

In this section we will comment on the relation of the observed physical properties to those measured in the wider fields of (i) aprotic ILs and (ii) glass-forming liquids in general. To commence, we consider the first-order phase changes, melting point and boiling point, and their relation to the internal cohesion indicator, T_g. This leads us to propose an energy level scheme within which the properties of these interesting liquids can be interpreted and which will later[21] be shown important for the interpretation of the properties of fuel cells containing these fluids as electrolytes. We discuss the transport properties, viscosity and conductivity, and their relationship to the ionicity of the liquids and to the possibility of "free" proton motion in electrolytes. The latter are all of importance to the possible applications of these liquids in such devices as fuel cells and photovoltaic converters. Finally we will examine how the protic IL fit into the overall "strong/ fragile" pattern of liquid viscosities, and how this may relate to the matter of "free" proton motion.

Melting Point−Glass Temperature Relations. It is common to relate the glass temperatures of glass-forming liquids to the melting points of the crystalline phase and obtain a linear relation with a slope close to 0.66 that has become known as the "$^2/_3$ law" for glass transition temperatures. This rule seems to apply quite well to the present study when a limited group of salts, related by cation type, is considered (as illustrated in Figure 7). However, when all salts, for which we have both glass temperatures and melting points, are examined without discrimination, the scatter around the ratio $^2/_3$ becomes rather large, see Figure 8, and it becomes apparent that the $^2/_3$ law is not at all precise. Indeed, such imprecision is expected on general grounds.

The scatter would be considerably worse if we were to include data on samples of the easily crystallizing liquids, when they have been vitrified by hyperquenching or by small sample techniques.

The imprecision of the $^2/_3$ law stems from the circumstance that the "law" is not due to any link between glass relaxation and melting mechanisms and is not a law for glass temperatures but, rather, is a way of predicting which members of a series of systems for which both T_g and T_m are known, will be slow to crystallize at normal cooling rates. They will be those whose melting points are less than 50% above their glass temperatures. If their melting points are too low, then the liquids will never crystallize and we will not find out what those melting points are. We will only know that they are much less than 1.5 T_g and that special efforts, involving possibly high-pressure methods, will be needed to find their crystalline states. The formate of propylammonium cation ($T_m = -75$ °C) must have one of the lowest melting points yet measured for an ionic liquid.

What are the factors involved in causing melting points to be so low, relative to the forces that determine the viscosity and glass temperature? These have been discussed by many authors, and the present results are consistent with many of the ideas that have been presented. Shape factors that lead to low packing efficiencies are prevalent among these ideas, the concept being that irregular packing can sometimes have advantages over ordered packing for minimizing the energy. This seems to be particularly true when there is more that one type of interaction to deal with. For instance when both hydrogen bonding and shape accommodation must simultaneously be satisfied, then it is generally more difficult to optimize in ordered arrangements. Thus, the cases for which no crystals form, according to the DTA scans, often have −OH groups on the asymmetric cations (hydroxypropylaminium cation, for example, does not yield crystals with any anions of our study). Empirically, the more viscous the liquid is at melting point, the higher the glass-forming tendency. A current study on a monatomic glassformer[28] reveals that glass-forming propensities are maximized when the competing crystalline phases have the same energy and the structure of the liquid is distinct from that of either possible crystal.

That the glass transition temperatures for PILs are generally lower than those of aprotic ILs of the same nominal charge concentration (L/equiv) was demonstrated in an earlier paper,[16] and this rule seems to be upheld in this more extensive study.

Boiling Points and T_b/T_m Relations. The implication that the cohesive energy of the PILs is below that of the corre-

TABLE 11: Thermal Transition Temperatures for Dihdrogen Phosphates

IL cation	symbol	T_g (°C)	T_c (°C)	T_m (°C)	T_b (°C)	ΔpK_a
Hydronium	$H_3OH_2PO_4$			21	158	-3.9
ammonium	$NH_4H_2PO_4$	−23.3	10	193.3	376.1[a]	7.1
methylammonium	MAH_2PO_4	−28.8	22.5	96.8	254.2[a]	8.5
ethylammonium	EAH_2PO_4	−31.3	−5.8	109.5	346.4[a]	8.5
propylammonium	PAH_2PO_4	n.d.[b]	n.d.	145.6	315.3[a]	8.4
butylammonium	BAH_2PO_4	−33.3	2.2	113.3	275.7[a]	8.5
methoxyethylammonium	$MOEAH_2PO_4$	−20.3	44.3	90.5	278.6[a]	7.3
dimethylammonium	$DMAH_2PO_4$	−36.8	15.1	117.3	245.3[a]	8.7
diethylammonium	$DEAH_2PO_4$	−16.7	13.3	159	330.0[a]	8.7
dibutylammonium	$DBAH_2PO_4$	−15.6	n.d.	98	316.7[a]	9.1
methylbutylammonium	$MBAH_2PO_4$	−36	n.d.	38.7	320.1[a]	8.8
trimethylammonium	$TMAH_2PO_4$	−36.7	n.d.	n.d.	274.4[a]	7.7
triethylammonium	$TEAH_2PO_4$	−32.2	n.d.	n.d.	349.2[a]	8.6
tributylammonium	$TBAH_2PO_4$	−18.8	n.d.	n.d.	337.5[a]	7.9

[a] Decomposes. [b] Not detected.

TABLE 12: Thermal Transition Temperatures for Difluorides

IL cation	symbol	T_g (°C)	T_c (°C)	$T_{S_1 \rightarrow S_2}$ (°C)	T_m (°C)	T_b (°C)	ΔpK_a	ΔpK_0[a]
ammonium	NH_4HF_2	n.d.[b]	n.d.	−33.1	125.6	240[c]	6.0	24.3
methylammonium	$MAHF_2$	−104.1	−72.5	−29.9	−11.8	174.5	7.4	25.7
ethylammonium	EA HF_2	−100.3	−67	−16	3.5	176.4	7.4	25.7
dimethylammonium	DMA HF_2	−111	−64.6	−37.2	−22.9	178.4	7.6	25.9

[a] The pKa value for hydrofluoric acid is taken as its Hammett acidity function value, $H_0 = -15.1$. [b] Not detected. [c] Decomposes.

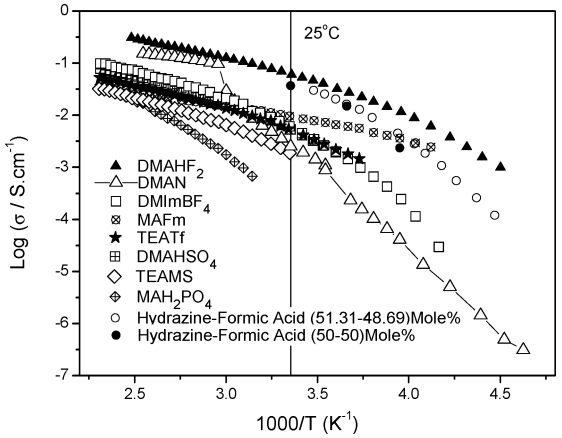

Figure 4. Ionic conductivities of a selection of the PILs from this study. In some cases, obvious from the breaks in the data, the conductivities of the crystalline states are included in the plot, as they have interesting high values.

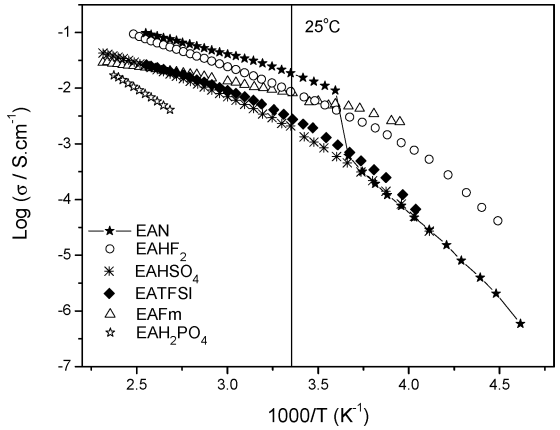

Figure 5. Ionic conductivities of PILs with a common cation (ethylammonium). The formate, with the weakest proton-transfer energy, shows distinct behavior.

sponding aprotic cases is supported by the boiling point data in Tables 3−12. Low T_g values generally correlate with low T_b values. Most of the salts that have high T_g values decompose before they can be observed boiling.

With molecular liquids, the boiling point/melting point ratio provides a reliable guide to glass-forming ability (GFA). Molecular liquids that boil at more than twice their melting points prove always to vitrify easily on cooling at normal rates. The present systems present an interesting test case here because, although the acid and base components are molecular liquids, their combination, on proton transfer, yields an ionic liquid in which the long-range coulomb forces might be expected to raise the boiling points sufficiently to invalidate the normal guide rule. The T_b/T_m ratio would then tend to exaggerate the GFA.

Although the majority of compounds reported here decompose before they boil, there are a number of cases in the Tables 3−5 where both boiling and melting points are available. For the formates, in which the proton transfer is not strongly driven (see below), the GFA is quite strong. This is predicted by the high T_b/T_m ratios, in some cases, but glasses also form in two cases where they are counterindicated by small (<2.0) ratios. Thus the expected enhancement of the GFA for these cases is not borne out in practice. On the other hand, the same small ratio (1.79) correctly predicts the weak GFA in the case of ethylammonium nitrate, for which the T_g could only be obtained by extrapolation of binary solution data. The failure of the fluoroacetates to yield GF liquids is also consistent with the low T_b/T_m ratios found for these compounds. Overall, then, the ionicities of these liquids do not seem to have led to failures of the common phenomenological rules for glass formers. Perhaps the extent of proton transfer needs to be greater than it is in these cases for the rules to break down as they do, for instance, with the alkali halides. (The eutectic temperature in the LiCl−KCl system, 685 K, is much less than half the boiling point, but there is no GFA at all.) For the cases of more energetic proton transfer, we cannot test the rule because decomposition occurs before the boiling point is reached.

Boiling Points and Proton-Transfer Free Energy Relations. The boiling point of a protic IL is strongly dependent on the extent of transfer of the proton from the acid to the base. In earlier work,[8] we linked the boiling point excess (excess over the value expected from simple additivity of the boiling points of acid and base components) to the difference in pK_a values

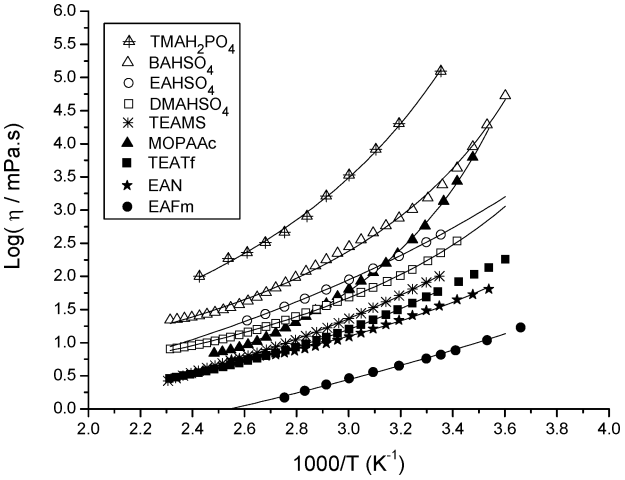

Figure 6. Viscosities of a selection of the PILs studied in this work. Data on others are available as Supporting Information.

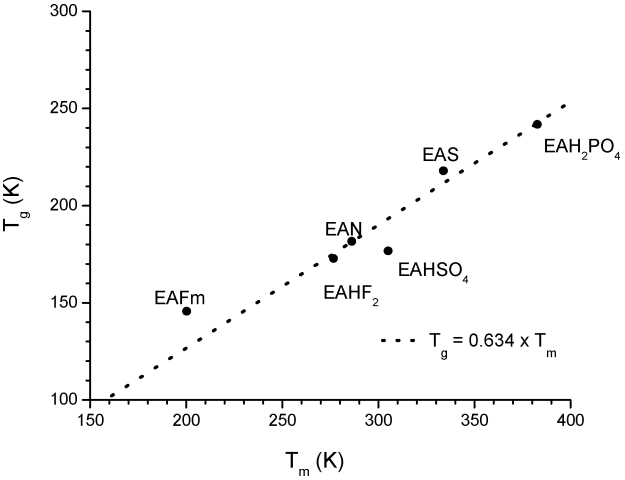

Figure 7. Melting point in relation to glass temperature for PILs in the ethylammonium family.

for the acid and base of the proton-transfer couple. Each individual pK_a value relates to the free energy of transfer of a proton from the Brönsted acid to the water molecule by the expression

$$\Delta G^0 = -RT \ln K_a \quad (1)$$

where K_a is the acid dissociation constant.

So the free energy of transfer of the proton from acid to base, in an aqueous environment, is the sum of the two free energies, thus

$$\Delta G^0 \text{ (acid-to-base)} = -RT\,\Delta \ln K_a$$

$$= -2.303RT\Delta pK_a \quad (2)$$

Below, we will use this relation of ΔpK_a value to the free energy of formation of the salt from the original acid and base by proton transfer (after rationalizing its use in the absence of water) to construct a free energy level diagram for the acids and bases of this work. From such a diagram, many properties of yet-unsynthesized proton-transfer IL can be predicted. First, however, we reinforce its relevance to the boiling process, i.e., to the process in which the original proton transfer is thermally reversed to restore the original acid and base molecules at a total vapor pressure of 1 atm. In Figure 9, we reproduce the figure from ref 8 to which we have now added new data

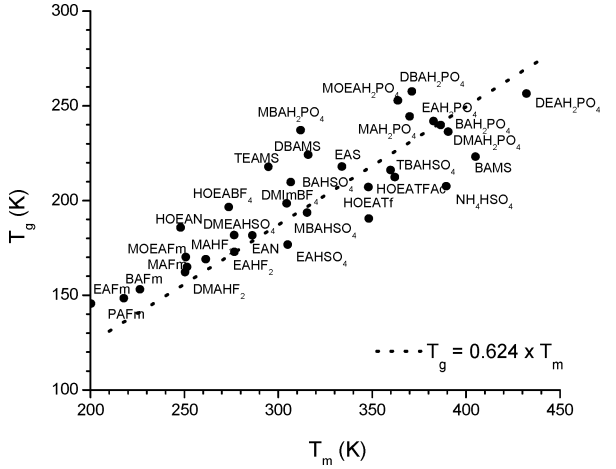

Figure 8. Melting point vs glass temperature for all PILs.

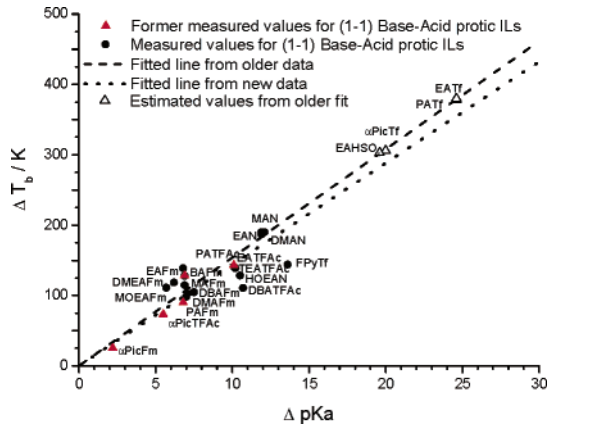

Figure 9. The "excess boiling point" of PILs in relation to the difference in acid and base pK_a values, from aqueous solution data. Solid points and dashed line are from ref 8. A maximum in the excess boiling point in an acid + base binary system will correspond to a maximum deviation from ideal mixing in an isothermal vapor pressure vs composition plot for each of the acid and the base at that composition. This can be converted to a measure of the free energy change on transfer of the proton from acid to base in the dielectric medium established by the neat IL. $\Delta G^0 = -RT\,\Sigma \ln p_i/2p^0_i)$ assuming this occurs at mole fraction = $^1/_2$. The quantity $2.303RT\Delta pK_a$ measures the free energy for the same process when the transfer occurs in the 1 M aqueous solutions. For strong monoprotic acids this will usually occur at the equimolar composition, though it may occur at higher X (acid) in cases where a strongly hydrogen-bonded dianion can form, as seen in an earlier study.[8]

acquired in the present study. The new data reinforce the earlier plot—so long as we restrict attention to proton transfers from acids to nitrogenous bases (which comprise the great majority of new data acquired in this study).

As seen before,[8] when the energy gap becomes larger than about 1 eV at 298 K, the boiling point becomes inaccessible because chemical decomposition (pyrolysis) occurs first. For those with less energetic proton transfers, the PILs can be evaporated under reduced pressure, and thereby purified or separated. They, and some unusual, strongly ion-paired aprotic IL cousins, have been called "distillable" ionic liquids.[29,30] On the other hand, protic ILs formed by proton transfers from superacids to strong bases behave like aprotic ILs.

It would be useful, in the future, to make direct vapor pressure measurements at lower temperatures (low vapor pressures) to clarify this domain of behavior (see also Figure 9 caption).

Gurney-Type Proton Free Energy Level Diagram for Proton-Transfer Systems. As indicated in the caption of Figure

9., the free energy change due to transfer of the proton from acid to base could be obtained from the appropriate vapor pressure measurements and a detailed comparison could then be made with the value estimated from the aqueous environmental data. Until this is done, however, the only comparison we can make is for the isolated cases where the appropriate free energy of formation ΔG_f^0 data for acid, base, and proton-transfer salt, are available in the literature. Let us check one case to see how serious the difference is. We take the case of ammonium nitrate for which the free energies of formation for NH_3, HNO_3, and NH_4NO_3 are tabulated in standard references. In such a case the free energy of formation of the proton-transfer salt from the acid and base components at 298 K can be obtained simply as

$$\Delta G^0 = \Delta G^0(NH_4NO_3) - \Delta G^0(HNO_3) - \Delta G^0(NH_3)$$

which proves to be −86.7 kJ/mol.[31] We convert the proton-transfer energy to units of electron volts, $\epsilon = -\Delta G^0/F$ (0.90 eV, only one proton is transferred) as used by Gurney in construction of the proton free energy level diagrams in his classic 1953 book, *Ionic Processes in Solution*.[32] The proton energy gap is therefore 0.90 eV.

Since ammonium nitrate, for which the free energy of formation is tabulated, is a solid, and since we are interested primarily in cases in which the product is a liquid, the above value should be corrected to one appropriate for the less stable supercooled liquid. The correct gap must therefore be smaller than 0.90 V. By knowledge of the entropy of fusion of ammonium nitrate (which we have measured:[33] −13.2 J/ mol· K at 443 K), we can assess the difference in free energy of liquid and crystal at the lower temperature, 298 K. It is small, amounting to only 1900 J. Corrected, the free energy change per mole of transferred protons is −85 kJ, and the "proton energy gap" that is crossed in forming the IL becomes 0.88 eV. These values are to be compared with those obtained from the thermodynamic data available for the free energies of formation of ammonium and nitrate ions from NH_3(aq) and HNO_3(aq).

For the process

$$NH_3(aq) + HNO_3(aq) \rightarrow NH_4^+(aq) + NO_3^-(aq)$$

the data yield a free energy change ΔG^0 of −50.3 kJ/mol, or 0.52 eV per transferred proton, rather different from those for the "dry" process. The 0.36 eV difference is due to differences in free energies of solution (to 1 M in water) of the three components of the above reaction, starting from their standard states.

The pK_a-based relation, eq 2 above, should give the latter value, but use of pK_a values for acids and bases in 1 M aqueous solution tabulated in standard sources[34] yields a larger value, 68.1 kJ/mol or 0.71 eV. There seems to be some uncertainty about the pK_a value to be assigned to HNO_3. HNO_3 dissociation was discussed in detail by Gurney and if we use his value of pK_a in the assessment we obtain a proton gap of 0.57 eV.

The differences in "wet" and "dry" values for the proton-transfer gap warn us that, irrespective of correlations such as that of Figure 9, the estimation of proton-transfer gaps from pK_a data is only semiquantitative. Because we lack direct measurements based on thermodynamic data such as vapor pressures, we will proceed semiquantitatively, using the pK_a values available in the standard sources and also in SciFinder Scholar, to construct a free energy level diagram for proton-transfer salts which will prove useful for predicting not only

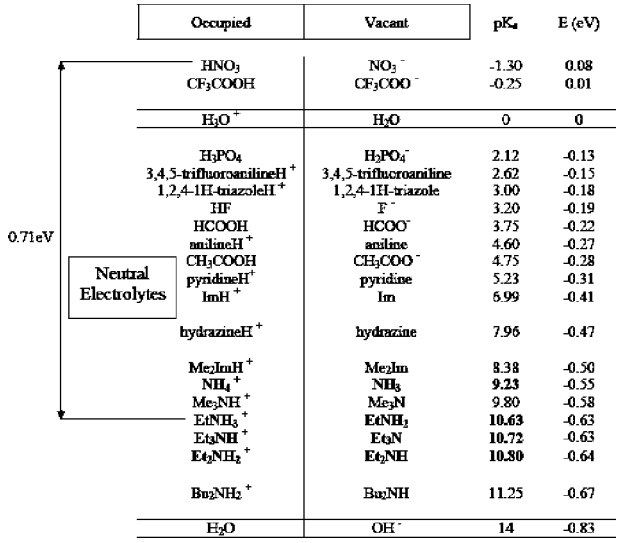

Figure 10. The proton free energy level diagram for ILs formed from moderately strong acid and moderately strong bases to yield neutral ionic liquid products. Arrows indicate the gap across which the proton falls in forming ethylammonium nitrate. Note that the value 0.71 eV is based on tabulated pK_a data and differs from the lower value, ∼0.52 eV, suggested by free energy data for NH_4NO_3 (aq).

excess boiling points and ionicities but also performance as electrolytes in hydrogen/oxygen fuel cells. The energy level diagram is closely related to that constructed by Gurney for 1 M aqueous solutions.[32] In Gurney's case, the only approximation involved was that of treating a one molar solution as a standard state.

The diagram is presented in two versions, one in which the levels are quantitative with respect to pK_a, but of limited range, and a second one in which the total range of energies is much larger and the relative placement of levels less precise. The advantage of the larger scale diagram is that it allows us to see how the commonly discussed acid electrolytes and also basic electrolytes, that have been used for two common types of fuel cells in the past, relate to the "neutral" electrolytes that we are now able to synthesize in great variety. What we will show separately[20] is that when the electrolyte is formed by dropping the proton across a specially favorable "gap," the properties of the electrolyte may be optimal from the point of view of maximizing the open circuit voltage of the fuel cell near the theoretical value.

Gurney's basic approach of pairing occupied and vacant proton energy levels was introduced in our earlier paper on proton-transfer Ils,[8] and now we utilize it here without duplicate explanation. Figure 10 shows the energy levels for the HNO_3/NO_3^- and NH_4^+/NH_3 conjugate pairs separated by the energy gap based on the difference in HNO_3 and NH_4^+ pK_a values tabulated in the CRC Handbook ($\epsilon = 2.303RT\Delta pK_a$). The values assigned to each level are based on an assignment of $\epsilon = 0$ eV to the H_3O^+/H_2O level. The other common level, that for H_2O/OH^-, lies at −0.83 eV from the reference level, based on the relation $pK_a(H_3O^+) + pK_a(OH^-) = 14$ (thus $\epsilon = \Delta G^0/F = -2.303RT(14/96\,500) = -0.83$ eV).

Between these levels are placed others for the couples HCOOH/$HCOO^-$, ethylammonium/ethylamine, triethylammonium/triethylamine, etc., while shortly above the H_3O^+/H_2O level we place the levels for medium strong acids, HNO_3/NO_3^- and CF_3COOH/CF_3COO^-, using in every case the tabulated pK_a values to quantify the levels.

With these levels assigned, and subject to the above "wet" vs "dry" free energy provisos, we can now immediately obtain

the proton-transfer energy involved in the formation of any ionic liquid that can result from combination of an acid in the left-hand column (an occupied proton level) with a base in the right-hand column (a vacant proton level), the proton-transfer resulting in the stable combination of anion and cation represented by the conjugate base and acid, respectively. [This uncertainty would be a much smaller value if the pK_a values could have been determined in an ideal solution state (a Henry's law standard state) in some particular ionic liquid solvent rather than in the usual aqueous solutions. This will be the subject of a separate publication (N. Byrne, J.-P. Belieres and C. A. Angell).] Thus we see that the formation of ethylammonium nitrate is accomplished by a proton falling across a gap of 0.71 eV or thereabout, which is close to the gap energy involved in the neutralization of H_3O^+ and OH^-. In the ethylammonium nitrate case, however, the resulting liquid consists of cations and anions, while in the case of water formation the product is a molecular liquid and an insulator.

Neutral Electrolytes vs Basic and Acidic Electrolytes. Ethylammonium nitrate, while highly ionic and conducting, has no acid or base properties, and relative to 1 molar acid or 1 molar base, it is a benign fluid. We call it a "neutral electrolyte" to distinguish it from a basic electrolyte, which is formed by transferring a proton from water to a strong base, e.g., to Na_2O to give the ionic product NaOH, which is highly corrosive when wet. Interestingly enough, according to the free energy change in the reaction $H_2O + Na_2O \rightarrow 2NaOH$, -143 kJ/mol, the proton crosses almost the same energy gap in forming "dry" NaOH as it does in the case of neutralization of 1 M strong acid with 1 M strong base, viz. 0.76 eV ($-\Delta G^0/2F$ because 2 mol of NaOH are produced). On the other hand, for NaOH(aq) the ΔG^0 value is more negative and the gap increases to 1.17 eV. For our purposes the "dry" value is the more appropriate. Thus the OH^-/O^{2-} level lies roughly the same distance below the H_2O/OH^- level as the latter lies below the H_3O^+/H_2O level. This is shown in the extended diagram, Figure 11.

We must note that the position of the OH^-/O^{2-} level on this diagram depends on how polarizing is the charge-compensating cation. By use of free energy of formation data, we obtain three levels for the three alkali metal cations Li^+, Na^+, and K^+. With Li^+, it falls at -0.54 eV, while for the less polarizing K^+ cation, it is lower, -1.03 eV. The properties of hydroxide solutions in which the alkali cations have been exchanged for weak field organic cations have not yet been explored to the best of our knowledge. Ionic liquid hydroxides presumably exist and they deserve study.

To understand the occurrence of decomposition before boiling in the case of PILs formed from superacids and strong bases, we need to add levels for the superacids to the energy diagram. To assign a level for triflic acid/triflate, we note that a pK_a of -14 has been assigned to triflic acid, based on the Hammett acidity function.[35] This leads us to place the HTf/Tf^- level 0.83 eV above the H_3O^+/H_2O level. Thus when ethylammonium triflate is formed, the proton drops 1.46 eV. The thermal energy required to place this proton back on the triflate ion to reform the molecule greatly exceeds the thermal stability of the ethylammonium group, so no boiling is observable. This PIL is as ionic as any aprotic IL. For the case of transfer to the weak base fluoropyridine, however, the proton gap is only 0.90 eV, and a boiling point is observable.

Note that the protic ionic liquid generated by the proton transfer from triflic acid to water is hydronium triflate. On the basis of the ΔpK_a values, the proton gap is 0.83 eV, coincidentally the same as for H_2O formation and for NaOH formation. The actual gap is likely lower, based on boiling point observations (see below). It is a remarkable observation, though, that NaOH concentrated aqueous solutions, hydronium triflate and its solutions in excess water, and ethylammonium nitrate, when used as electrolytes in fuel cells, all yield cells that have the theoretical open circuit voltage for the H_2/O_2 reaction producing water. In a separate paper we will examine the question of whether or not this is just coincidence.

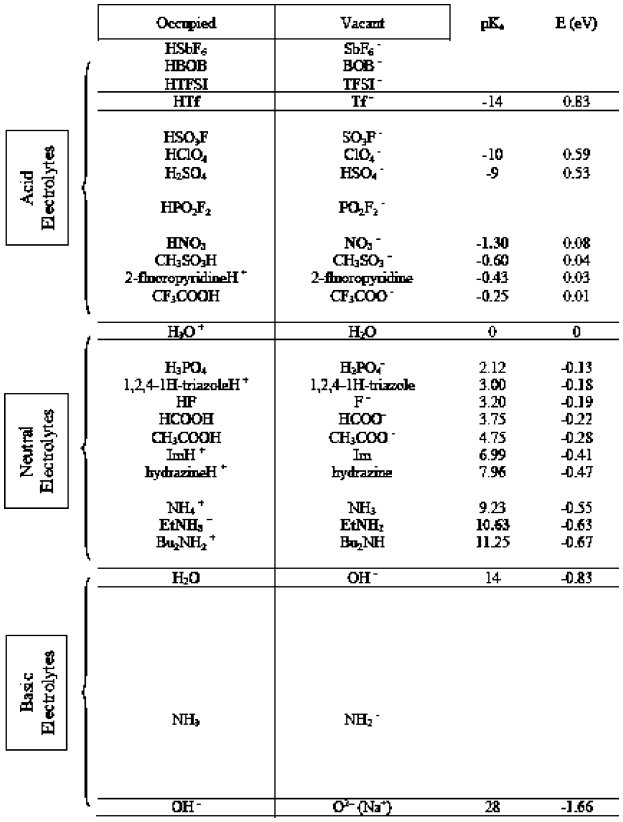

Figure 11. Full proton free energy level diagram, showing the levels between which the proton falls in forming acid electrolytes as well as those between which it falls in yielding the basic electrolytes of familiar fuel cells.

Nitrogenous vs Oxygenous Bases. It might be expected from the latter observations concerning the proton gap that the excess boiling point for hydronium triflate would be similar to that found for ethylammonium nitrate and its cousins. To our surprise this proves not to be the case. In the four studied instances of proton transfers to the water molecule, the excess boiling point can be measured, and the increase in boiling point is smaller than for the nitrogenous base cases of equal ΔpK_a values. With only four points and considerable scatter, a figure is unwarranted, but whatever the reason, it is clear that the stabilization of the liquid against reversion to the original base and acid molecular liquids is much smaller with oxygenous bases than is indicated by the tabulated ΔpK_a values.

Transport Properties and Ionicity

We now turn to the transport properties, conductivity, and fluidity. Generally speaking the liquids with high conductivities are also those with high fluidities, indeed this would be expected from the Walden rule connecting the charge mobility to the frictional resistance to its motion offered by the liquid viscosity, η. We have used the plot of $\log \Lambda$ vs $-\log \eta$ (i.e., $\log \Phi$, where Φ is the fluidity) in a number of previous papers to classify ILs into ideal, subionic, and superionic cases, with most interest residing in the latter.

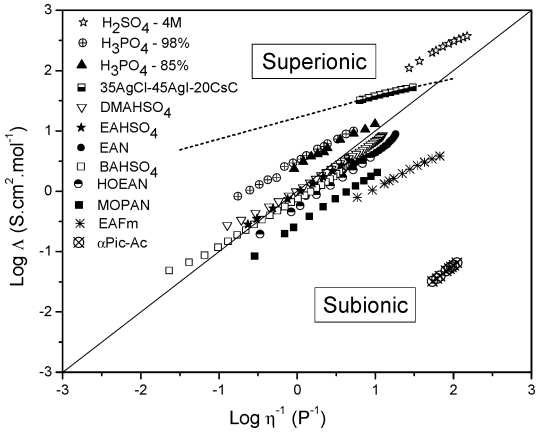

Figure 12. Walden plot for a selection of ILs of this study, for α-picolinium acetate from ref 8 and for a silver ion superionic from ref 16.

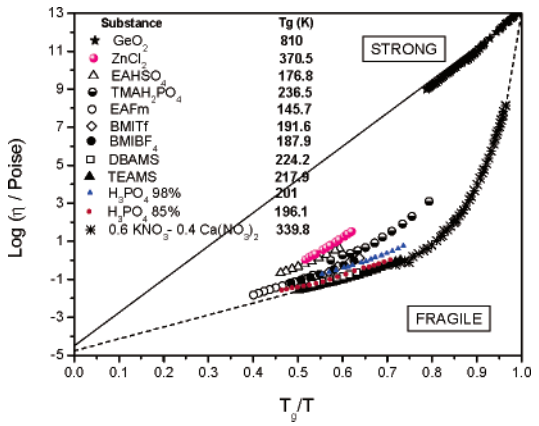

Figure 13. Fragility plot for a selection of ILs of this study. Note the presence of the dihydrogen phosphates, which support superprotonic conductivity, in the intermediate fragility domain. Hydrated phosphoric acid, the best free proton conductor, is however, not an intermediate liquid in this scheme.

One of the hopes for this study was that, by covering a broad enough range of systems, cases in which the transferred protons would find ways of moving through the fluid independently of the bulkier anions and cations might emerge. Certainly a "dry" proton conductivity mechanism is one of "holy grails" of electrolyte science. Such cases could be revealed by means of the classical Walden plot, "dry" proton motion being indicated by data points in the "superionic" domain of the diagram above the diagonal line of unit slope. So far we have little indication of such a mechanism, though it does seem to be significantly present in the case of phosphoric acid, especially at very high concentrations where the standard Grotthus mechanism that acts in the case of dilute aqueous acids has been largely suppressed by breakdown of the water network.

Walden plots for a number of cases from the present study are shown in Figure 12. Some data for phosphoric acid of high concentration and sulfuric acid at low concentration are included as examples of superionic behavior. We note that the mole ratio of water to phosphoric acid is very close to unity in the 85 wt % H_3PO_4 solution. If there were a substantial proton energy level gap between $H(H_2PO_4)/H_2PO_4^-$ and H_3O^+/H_2O, then 85% H_3PO_4 would be hydronium dihydrogen phosphate, but in fact the gap is negative. The subject of such acidic solutions, as opposed to PILs, will be dealt with in a separate paper.

While superionic conductivity is regrettably not in evidence in the protic ILs of the present study, the opposite case of "subionic" conductivity is abundantly illustrated. For any case in which the proton-transfer energy, according to Figure 11, is less than 0.5 eV, we find conductivities well below the ideal line of Figure 12. They did not yield the conductivity expected from their high fluidities because on average the proton transfer is incomplete.

They behave as if there is only a small population of ions and the "ionicity" of the liquid is therefore reduced, i.e., the liquid is subionic. Data from a subset of the cases studied are shown in Figure 12 to illustrate this point. It was shown in Figure 10 of our previous paper[8] that the deviation from Walden ideality varies very strongly with ϵ at low ϵ but then flattens out and becomes insignificantly different from the ideal value for any $\Delta pK_a > 8$ ($\epsilon > 0.5$ eV). The present study confirms this finding but adds little to it. It is confirmed, then, that for purposes of electrical conductivity, any moderately large ϵ (>0.6, suffices to give IL conductivity) but low vapor pressure requires the largest possible proton energy gap. The volatility of low-gap PILs has been noted in other recent publications.[29,30] The present article provides a basis for predicting the volatility in individual cases.

Fragility of PILs. Finally we return to the starting point of this article to ask where the liquids of this study fall in relation to the simple molten salts, including many aprotic ILs, with respect to the important liquid-state property, fragility, i.e., where do they fall in the overall hierarchy of configurational excitability. Although we have not made viscosity measurements over a very wide range, there are enough data to provide an adequate idea of their range of behavior.

In Figure 13, we plot the data for the present liquids within a frame provided by the most, and least, fragile of the aprotic ILs. We include one "intermediate" case, that of the dense (as opposed to open) network liquid, zinc chloride. It can be seen that the PILs cover the spectrum from intermediate to very fragile, with strong representation in the intermediate range from the cases with acid anions.

These are the cases which have greatest hydrogen-bonding contributions to their interparticle interactions and which will therefore tend to have most extended intermediate range order. Intermediate range order is a characteristic associated with low fragility. Perhaps not surprisingly, the dihydrogen phosphates are also the cases in which evidence for superprotonic behavior is strongest (see Figure 12).

Concluding Remarks

The protic subclass of ILs is enormously broad, and we have only touched on the most obvious examples. There is a very large group of PILs with benign and even edible cations, and complimentary anions, with biologically interesting possibilities waiting to be explored. It is common knowledge that many pharmaceutical preparations are marketed as "hydrochlorides". These are proton transfer salts chosen for their high melting points. Many would become PILs if the chloride anion was replaced by thiocyanate or trifluoroacetate. On the other hand, there is a smaller field of inorganic protic ILs some members of which have proven of great interest as electrolytes for fuel cells.[40] While examples of single component inorganic protic salts with melting points below 100 °C (like hydrazinium nitrate (T_m = 70 °C)[27,41] may be rare, mixtures of such salts are frequently liquid in the IL range, and their stabilities, in the case of large proton transfer energies, may be important.[40]

Acknowledgment. This work has been carried out under the auspices of the DOD-Army Research Office and NASA,

under Grant Nos. W91FF-04-1-0060 and NNC04GB068, respectively. The authors wish to thank Dr. Cristina Iojoiu for the Karl Fisher titration and Dr. Nolene Byrne for her assistance with the NMR spectra. The authors also wish to thank two former group members for their help, Dr. Wu Xu and Dr. Fuminori Mizuno.

Supporting Information Available: Density and molar volume data and viscosities of some PILs studied in this work. This material is available free of charge via the Internet at http://pubs.acs.org.

References and Notes

(1) Davy, H. *Experimental researches in electro-chemistry: including the Bakerian lectures, and memoirs read before the Royal Society, on the chemical agencies of electricity, and on the metals of the alkalies and earths*; Griffin, J. J. and Griffin, R.: London, 1848.

(2) Angell, C. A.; Xu, W.; Yoshizawa, M.; Hayashi, A.; Belieres, J.-P.; Lucas, P.; Videa, M. In *Electrochemical Aspects of Ionic Liquids*; Ohno, H., Ed.; Wiley-Interscience: 2005; p 5.

(3) Angell, C. A. *J. Phys. Chem.* **1966**, *70*, 2793.

(4) Wasserscheid, P.; Welton, T. *Ionic Liquids in Synthesis*; Wiley-VCH, 2003.

(5) *Ionic Liquids: Industrial Applications to Green Chemistry*; Rogers, R. D., Seddon, K. R., Eds.; American Chemical Society, 2002.

(6) Wang, P.; Zakeeruddin, S. M.; Humphry-Baker, R.; Gratzel, M. *Chem. Mater.* **2004**, *16*, 2694.

(7) Susan, M. A. B. H.; Noda, A.; Mitsushima, S.; Watanabe, M. *Chem. Commun.* **2003**, 938.

(8) Yoshizawa, M.; Belieres, J. P.; Xu, W.; Angell, C. A. *Abstracts of Papers of the American Chemical Society* **2003**, *226*, U627.

(9) Walden, P. *Bull. Acad. Imper. Sci.* **1914**, *405*.

(10) Reinsborough, V. C. *Rev. Pure Appl. Chem.* **1968**, *18*, 281.

(11) (a) Gruen, D. M.; McBeth, R. L. *Pure Appl. Chem.* **1963**, *6*, 23. (b) Gruen, D. M.; McBeth, R. L. *J. Phys. Chem.* **1959**, *63*, 383.

(12) Easteal, A. J.; Angell, C. A. *J. Phys. Chem.* **1970**, *74*, 3987.

(13) Hirao, M.; Sugimoto, H.; Ohno, H. *J. Electrochem. Soc.* **2000**, *147*, 4168.

(14) Ohno, H.; Yoshizawa, M. *Solid State Ionics* **2002**, *154*−*155*, 303.

(15) Yoshizawa, M.; Ohno, H. *Chem. Commun.* **2004**, 1828.

(16) Xu, W.; Angell, C. A. *Science* **2003**, *302*, 422.

(17) Yoshizawa, M.; Xu, W.; Angell, C. A. *J. Am. Chem. Soc.* **2003**, *125*, 15411.

(18) Kreuer, K. D.; Fuchs, A.; Ise, M.; Spaeth, M.; Maier, J. *Electrochim. Acta* **1998**, *43*, 1281.

(19) Susan, M. A. B. H.; Yoo, M.; Nakamoto, H.; Watanabe, M. *Chem. Lett.* **2003**, *9*, 836.

(20) Belieres, J.-P.; Gervasio, D.; Angell, C. A. *Chem. Commun.* **2006**, 4799.

(21) Belieres, J.-P.; Xu, W.; Markusson, H.; Gervasio, D.; Angell, C. A. To be published.

(22) Evans, D. F.; Kaler, E. W.; Benton, W. J. *J. Phys. Chem.* **1983**, *87*, 533.

(23) Mao, O.; Altounian, Z.; Strom-Olsen, J. O. *Rev. Sci. Instrum.* **1997**, *68*, 2438.

(24) Videa, M. Conductivity and self-diffusivity measurements on molten lithium electrolytes for battery applications. Ph.D. Thesis, Arizona State University, 1999.

(25) Noda, A.; Susan, M. A. B. H.; Kudo, K.; Mitsushima, S.; Hayamizu, K.; Watanabe, M. *J. Phys. Chem. B* **2003**, *107*, 4024.

(26) Belieres, J.-P. Protic Ionic Liquids, High Temperature Electrolytes for Fuel Cell Applications. Ph.D. Thesis, Arizona State University, 2005.

(27) Sutter, E. J. Hydrogen Bonding and Proton Transfer Interactions in Hydrazine-Based Binary Liquids and Related Systems. Ph.D. Thesis, Purdue University, 1970.

(28) Molinero, V.; Sastry, S.; Angell, C. A. *Phys. Rev. Lett.* **2006**, *97*, 075701/ 1.

(29) Earle, M. J.; Esperanca, J. M. S. S.; Gilea, M. A.; Canongia Lopes, J. N.; Rebelo, L. P. N.; Magee, J. W.; Seddon, K. R.; Widegren, J. A. *Nature* **2006**, *439*, 831.

(30) MacFarlane, D. R.; Pringle, J. M.; Johansson, K. M.; Forsyth, S. A.; Forsyth, M. *Chem. Commun.* **2006**, *18*, 1905.

(31) Atkins, P. W. *Physical Chemistry*, 6th ed.; 1997.

(32) Gurney, R. W. *Ionic Processes in Solution*; Dovers Publications: New York, 1962.

(33) Belieres, J.-P.; Angell, C. A. Unpublished Work, 2005.

(34) The pK_a values were taken from (a) Covington, A. K.; Davison, W. *CRC Handbook of Chemistry and Physics*, 75th ed.; Lide, D. R., Ed.; Chemical Rubber Co. Press: Boston; p 8−43 and (b) *Lange's Handbook of Chemistry*, 13th ed.; Dean, J. A., Ed.; McGraw-Hill, Inc.: New York; p 5−18. For the case of triflic acid, we adopted the pK_a value −14 suggested by Ripin and Evans (see http://daecr1.harvard.edu/pKa/pKa.html).

(35) Hammett, L. P.; Deyrup, A. J. *J. Am. Chem. Soc.* **1932**, *54*, 2721.

(36) Sacco, A.; Belorizky, E.; Jeannin, M.; Gorecki, W.; Fries, P. H. *J. Phys. II* **1997**, *7*, 1299.

(37) Yoshizawa, M. Design and Characteristics of Ionic Liquids Featuring Target Ion Transport. Ph.D. Thesis, Tokyo University of Agriculture and Technology, 2001.

(38) Xu, W.; Angell, C. A. Unpublished Work, 2004.

(39) Sare, E. J. Structure and Bonding Investigation of Aqueous Electrolyte Solutions by PMR Spectroscopy and a New Diagnostic Tool—The Glass Transition Temperature. Ph.D. Thesis, Purdue University, 1971.

(40) Belieres, J.-P.; Gervasio, D.; Angell, C. A. Binary inorganic salt mixtures as high conductivity electrolytes for >100 °C fuel cells. *Chem. Commun.* **2006**, DOI: 10.1039/b611150e.

(41) Sutter, E. J.; Angell, C. A. *J. Phys. Chem.* **1971**, *75*, 1826.